

## MAGNETIC NANOPARTICLES GENERATED BY LASER ABLATION IN LIQUID

G. BULAI<sup>a\*</sup>, I. DUMITRU<sup>a</sup>, M. PINTEALA<sup>b</sup>, C. FOCSA<sup>c</sup>, S. GURLUI<sup>a</sup>

<sup>a</sup>*Faculty of Physics, Alexandru Ioan Cuza University of Iasi, 700506 Iasi, Romania*

<sup>b</sup>*Centre of Advanced Research in Bionanoconjugates and Biopolymers, Petru Poni Institute of Macromolecular Chemistry, 41A Gr. Ghica Voda Alley, 700487 Iasi, Romania*

<sup>c</sup>*Laboratoire de Physique des Lasers, Atomes et Molécules (UMR 8523), Université Lille 1 Sciences et Technologies, 59655 Villeneuve d'Ascq, France*

We report on the generation of magnetic nanoparticles by nanosecond laser ablation of cobalt ferrite in liquid. We investigated the influence of both ablation liquid (water, ethanol, polyethylene glycol in water) and irradiation conditions (laser energy/pulse and spot size) on the nanoparticles dimension, shape, structure, chemical composition and magnetic properties. A single phase cobalt ferrite target was immersed in various solutions and irradiated with an Nd-YAG laser at fluences varying from 4 to 12 J/cm<sup>2</sup>. A first characterization of the so generated colloidal solution was performed by UV-VIS absorption spectroscopy. Then, the samples were dried at 80 °C and the resulting material was collected for further investigations. The structural and chemical properties were studied by X-ray diffraction (XRD), transmission electron microscopy (TEM) and scanning electron microscopy/energy dispersive X-ray spectroscopy (SEM/EDX). The nanoparticles magnetic response was recorded using a vibrating sample magnetometer (VSM). TEM micrographs revealed that the particle diameter and size distribution varied as the laser energy and irradiation spot area were modified or when polymer surfactant was added to the ablation liquid. The broad absorption band observed for all analyzed solutions was considered to be a superposition of multiple peaks associated to iron oxides. EDX measurements revealed an overstoichiometry of iron for most samples. VSM results confirmed the ferromagnetic character of the nanoparticles and their magnetic parameters were correlated to their size and chemical composition.

(Received February 3, 2016; Accepted March 21, 2016)

*Keywords:* nanoparticles, laser ablation, polyethylene glycol, TEM images

### 1. Introduction

Magnetic materials have attracted significant attention in the last few decades due to their interesting properties and technological significance in developing new systems and improving the performances of existing materials. Among these, ferrites are considered to be an important class of materials which are used extensively in magnetic data storage, sensors, actuators, wave guides etc. [1-3]. Moreover, the applicability domain of the spinel ferrites can be extended when relating to nanostructured forms such as thin films and nanoparticles [4-7]. Each potential application of the magnetic nanoparticles relies on specific properties. For data storage applications, the particles need to present a stable and switchable magnetic state. It is important that these structures preserve their ferromagnetic characteristic, considering that as their dimensions are decreased the nanoparticles can turn to a superparamagnetic state with zero coercivity and no remanent magnetization. For therapeutic applications (such as hyperthermia) the use of subdomain magnetic particles is preferred over multidomain particles, as they can absorb much more power at tolerable

---

\* Corresponding author: georgiana.bulai@uaic.ro

AC magnetic fields. The synthesis of uniform nanoparticles with narrow size distributions can offer a rigorous control in temperature [8].

The combination of cobalt ferrite (both in thin film and nano-powder forms) with polymer materials can account for significant advances in different technological areas such as flexible electronics, magnetic resonance imaging (MRI), drug delivery, microwave frequency transducers, multiple state memory elements, highly transparent magneto-optic materials, magnetic field sensors etc. [6,9-11]. The magnetic characteristics of magnetic nanoparticles – polymer composites can be changed by varying different external factors (e.g. temperature, magnetic field), thus by changing the distances between particles [12]. The optic and magnetic response of these transparent nanocomposites depends significantly on the dimension, shape and structure of the nanoparticles.

Pulsed laser ablation is a method that can ensure the formation of thin films with specific properties and also the synthesis of nano-sized particles with crystalline structure, no segregation and/or agglomeration and large magnetic response. Laser ablation in liquid (LAL) can offer extreme conditions of pressure (~ 1 GPa) and temperature (~6000 K) so that metastable structures with novel properties can be obtained [13]. Compared to chemical methods, LAL presents several advantages such as: a) variety of materials which can be obtained and of liquid solutions which offer a stable handling of the colloids; b) high purity of the nanoparticles by avoiding the use of chemical ligands or reducing agents; c) controllable size and shape [14,15].

LAL was successfully used to synthesize metal nanoparticles (Fe, Co, Pd, Cu, Au, Ag, W, Al) [16-21], but also more complex materials ( $\text{MnFe}_2\text{O}_4$ ,  $\text{NiFe}_2\text{O}_4$ ,  $\text{SrFe}_{12}\text{O}_{19}$ ,  $\text{Mn}_3\text{O}_4$ ) [22-24]. Nanostructures with compositions different from the source material were synthesized by controlling the chemical reactions between the target and liquid solution. Maneeratanasarn et al. [25] showed that single phase iron oxide can be obtained in different types of solvents by modifying the target composition as well as the laser irradiation conditions. Desarkar et al. [26] observed that higher laser fluence leads to the formation of smaller particles. Moreover, as the ablation time increases, the number of particles increases initially and then saturates due to the shielding of the incident laser radiation by the formed nanoparticles.

In the continuity of our previous works [27,28] on the synthesis of low-dimension structures by laser ablation of cobalt ferrite (pure or rare-earth doped), we performed a study on the generation of magnetic nanoparticles by laser ablation in liquid, with the aim of investigating the influence of the ablation liquid and laser irradiation parameters on the particles properties. The paper presents the main results of this study, with special focus on the structural, chemical and magnetic properties of the cobalt ferrite nanoparticles generated by laser ablation in liquid.

## 2. Experimental details

Cobalt ferrite bulk material was synthesized by standard ceramic technique. Commercially available  $\text{Fe}_2\text{O}_3$ ,  $\text{Co}_3\text{O}_4$  oxides were mixed in adequate proportions, calcined and ball milled. The final sintering process was done at 1250 °C for 5 h at 100 °C/h heating rate followed by natural cooling to room temperature. A more detailed presentation of the preparation process is given in [29]. The ablation targets were manufactured by pressing the cobalt ferrite powders into disks at 250 MPa and then placed at the bottom of a glass vessel, in 40 ml liquid volume. Various ablation liquids were used: ethanol, distilled water and a solution of polyethylene glycol (PEG, MW=6000) in distilled water at three different concentrations. The target irradiation was done at normal incidence using the second harmonic (532 nm) of an Nd-YAG laser with 10 Hz repetition rate and 10 ns pulse duration. The laser energy/pulse was varied from 40 mJ to 80 mJ and the irradiated surface changed from 0.63 mm<sup>2</sup> to 2 mm<sup>2</sup>, resulting in ablation fluences in the range 3 - 12.5 J/cm<sup>2</sup>. Seven samples (denoted N1-N7 in the following) were so generated using the specific experimental conditions summarized in Table 1.

Table 1. Experimental conditions used for nanoparticle synthesis, parameters of log-normal fit of TEM histograms, chemical composition (EDX) and magnetic parameters (VSM).

Sample	Ablation liquid	Energy (mJ)	Ablation spot area (mm <sup>2</sup> )	Fluence (J/cm <sup>2</sup> )	Mean particle diameter (nm)	Standard deviation	Fe:Co ratio EDX	H <sub>c</sub> (kOe)	m <sub>r</sub> /m <sub>max</sub>
					log-normal fit				
N1	Distilled water	60	0.63	9.5	22.9	1.3	-	-	-
N2	Distilled water	80	0.63	12.5	-		3.07	0.75	0.17
N3	Distilled water	40	0.63	6.3	22.8	1.4	2.97	1.19	0.53
N4	Distilled water	60	2	3	19.5	1.3	2.37	0.64	0.16
N5	Distilled water + PEG (0.09mM)	60	0.63	9.5	16.6	1.2	1.5	0.94	0.27
N6	Distilled water + PEG (0.05mM)	60	0.63	9.5	17.1	1.3	2.75	1.33	0.47
N7	Ethanol	80	0.63	12.5	26.8	1.2	2.87	-	-

UV-VIS absorption spectroscopy was first performed on the obtained colloids using a UV-VIS-NIR source DT-MINI-2-GS coupled with an Ocean Optics spectrometer QE65000. The structural and chemical properties of the nanoparticles were analyzed by X-ray diffraction (Shimadzu LabX XRD-6000 advanced diffractometer with a Cu-K $\alpha$  radiation ( $\lambda=1.5406$ ), standard mode), transmission electron microscopy (TEM, LVEM5 Benchtop Electron Microscope), scanning electron microscopy and energy-dispersive X-ray spectroscopy (SEM/EDX, Vega Tescan LMH II microscope and Bruker AXS Microanalysis GmbH detector). For TEM analysis, solution drops from each sample were dried on Cu grids. The SEM/EDX measurements were done on solution deposits on carbon strips and the chemical composition was obtained by analyzing 1  $\mu\text{m}$  x 1  $\mu\text{m}$  surfaces. For XRD measurements the solutions were dried on glass substrates at a temperature of 80°C. The magnetic characteristics were investigated using a Vibrating Sample Magnetometer (VSM, Princeton/Lakeshore M3900). For this measurement, fragments of 5 mm x 5 mm of dried nanoparticle deposits were analyzed.

### 3. Results and discussions

The morphology and size distributions of the nanoparticles synthesized by laser ablation were investigated by TEM imaging. Figure 1 presents the histograms obtained by analyzing the observed nanoparticles for each of the N1-N7 samples, while the insets show the corresponding TEM micrographs. The histograms were fitted using a log-normal function (red line) and the resulting parameters (main particle diameter, standard deviation) are listed in Table 1. Most particles are spherical and have diameters ranging from 16 to 27 nm (see Table 1) with an asymmetric size distribution. TEM images also showed some particles as large as 100 nm (see inset Figure 1, N3 sample) and also agglomerations that occur after the laser irradiation process. The magnified images of the investigated nanoparticles revealed that the cores have higher electron densities compared to the grey outer layers indicating a change in composition and in structural characteristics. A TEM image of such a particle is given in the inset of Figure 1 for the N5 sample. We suppose that the aqueous medium in which these cobalt ferrite nanoparticles were generated, together with their high reactivity, led to the formation of magnetic nanoparticles covered by an oxide shell.

The oxidation of cobalt and iron nanoparticles (as well as of other metals: Cu, Mg, Sn) obtained by laser ablation in water was observed by other research groups as well [19,24,30,31]. Composition changes can occur due to the photochemical and thermal processes that take place during laser ablation and which depend on the properties of the investigated material and of the solution. Tsuji et al. found that Co<sub>3</sub>O<sub>4</sub> oxide can come from the chemical reaction between Co and

O obtained by photodecomposition of cobalt oxide and water, respectively, or from photothermal processes that take place due to the high temperatures involved [19]. Liu et al. obtained FeO from iron plate ablation in water by subsequent decomposition of Fe-(OH)<sub>2</sub> nanoparticles at high temperature and high pressure which are associated with the liquid confined plasma [30]. Smaller nanoparticles (below 20 nm mean diameter) with narrower size distribution and fewer agglomerations were obtained when PEG surfactant was added. This result is in agreement with other reported studies in which PEG was used to disperse the obtained nanoparticles. With PEG addition, a thin layer of polymer is formed on the surface which effectively shields the surface charge of the nanoparticles thus preventing their agglomeration [32-34]. However, as the concentration of the PEG surfactant was increased from 0.05 mM to 0.09 mM, no significant changes in size distribution were observed, possible due to the low variation of dissolved PEG mass.

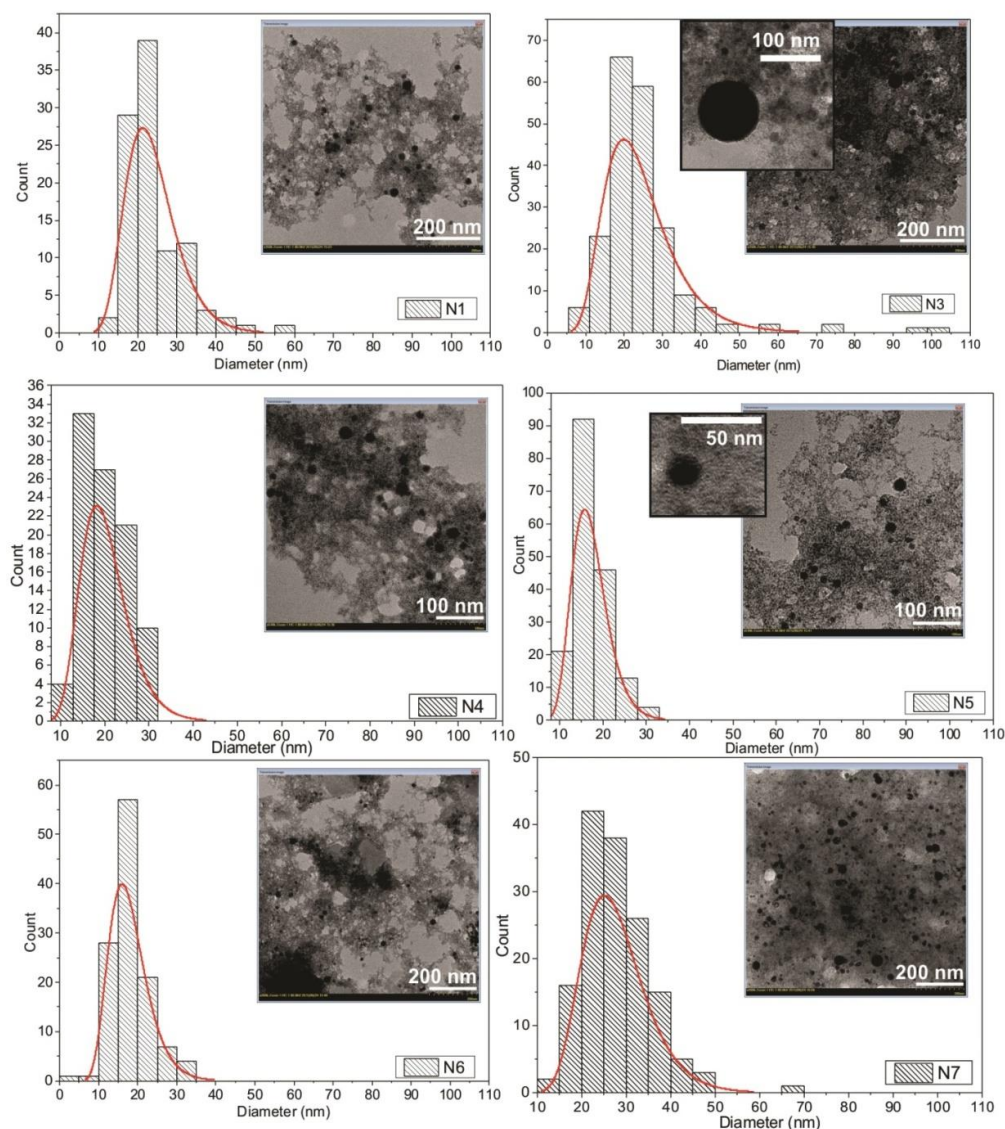


Fig. 1. Histograms and TEM images of the nanoparticles obtained by laser ablation in various conditions (see Table 1); the red lines represent the log-normal fit of the histograms

The increase of laser energy/pulse from 40 mJ to 60 mJ on the same irradiation surface (0.63 mm<sup>2</sup>) determined the formation of solution with fewer large particles as observed from the histograms presented in Figure 1 (comparing the N3 and N1 samples). Moreover, the mean particle diameters from lognormal fit for both solutions were found to be around 23 nm. Thus, the

use in this study of a higher energy did not determine a decrease in mean particle size but rather a narrower size distribution. In their study on palladium nanoparticles, Nishi et al. [17] reported that for short time laser ablation (several minutes) the fluence variation contributes to differences in ablation rate and also on the size distribution. After several minutes the laser energy reaching the target surface is decreased due to the shielding effect of the generated nanoparticles. The incident energy leads to a higher kinetic energy of the ejected nanoparticles and increases the collisions between them. As a consequence, the initially formed large particles undergo fragmentation processes which further reduce their dimension and make the size of each particle relatively uniform [35]. Furthermore, a narrower size distribution but also a slight reduction in nanoparticle size was observed when the area of the irradiated surface was increased from  $0.63 \text{ mm}^2$  to  $2 \text{ mm}^2$ . A decrease in particle size was observed by Sobhan et al. in their study on the influence of spot size on the morphology of gold nanoparticles [36]. The use of a smaller laser spot size favors droplets or large particle emission [37]. This is also consistent with observations related to laser ablation in gaseous media where the use of a larger spot size determined a decrease in large particle deposition (droplet density) on the surface of thin films [38].

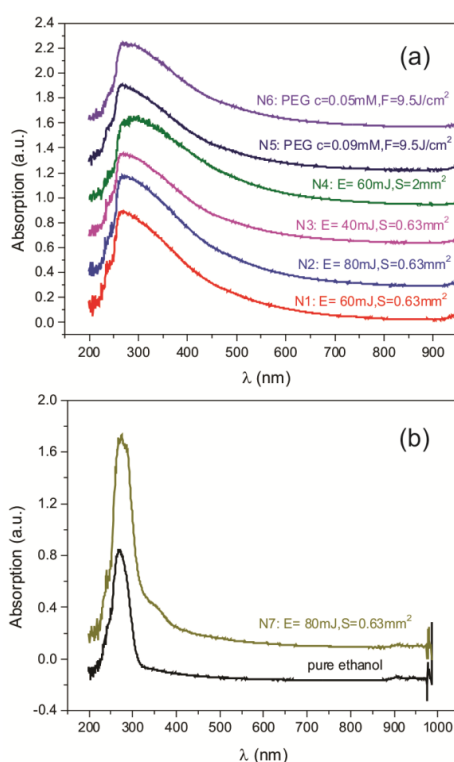


Fig. 2. UV – VIS absorption spectra of cobalt ferrite nanoparticles obtained in (a) water and (b) ethanol

Fig. 2 presents the LAL-generated colloids UV-VIS absorption spectra in the 200 nm – 1000 nm wavelength range. The spectrum recorded for distilled water (not shown) did not present any significant features in this spectral domain, unlike the one of ethanol where a peak at 270 nm is present (see Figure 2b, bottom curve) and can affect the interpretation of the N7 solution spectra. The absorption spectra of the cobalt ferrite nanoparticles generated in distilled water and in distilled water and PEG mixture present a wide band from 220 nm to 520 nm with maxima around 265 nm (Figure 2a). The changes in peak position and in its shape can give information related to modifications in particle size and also in particle morphology. An increase of the particle diameter can determine a red shift of the absorption peak [26,39]. However, in this study, no significant variations were found as the irradiation conditions used for particle generation were modified. Although TEM results present changes in particle dimension and size distribution, it appears that these changes were not enough to significantly influence the absorption spectra. Rajesh et al. [40] observed two peaks at 280 nm and 307 nm for the  $\text{Fe}_3\text{O}_4$  nanoparticles prepared

by chemical process. The peak at  $\sim 270$  nm was reported for solutions of metal iron nanoparticles and was further confirmed through calculations with Mie model [41]. Slightly modified spectrum was observed for the N4 sample for which the maximum absorption seems to be shifted towards 300 nm, instead of 265 nm. This result can be explained by the lower laser fluence used for particle generation which could decrease the oxidation process rate. The absorption spectra of the nanoparticles formed in ethanol present a peak at 350 nm which can also be associated with iron oxide. The broad absorption band can be a result of the superposition of several peaks as observed by Klačanová et al. [42] when studying iron nanoparticles in water. Under inert atmosphere, the absorption spectra presented two peaks at 262 nm and 352 nm. On keeping the sample under air, new absorption bands appeared indicating various oxide nanoparticles (369 nm, 430 nm, 487 nm). Our UV-VIS spectroscopy measurements indicate that the solution consists more of iron oxide nanoparticles rather than cobalt ferrite, which, according to literature [43], would give a peak around 300 nm. This result is also supported by EDX measurements which indicate that there is an overstoichiometry of Fe in the samples. In most cases, the Fe:Co ratio (see Table I) is higher than the stoichiometric value of 2:1.

Further structural study was done using X-ray diffraction. For this analyzing step the nanoparticles were dried on amorphous glass substrate at a temperature of  $80^\circ\text{C}$  to avoid the evaporation of the added surfactant. The XRD patterns did not present any diffraction lines indicating that the laser ablated nanoparticles were amorphous. However, the absence of diffraction lines can be also a result of the small amount of analyzed material. The main disadvantage of LAL is the relatively low product yield. An exception was observed for the N2 sample for which weak diffraction peaks were recorded (Figure 3). The use of a high fluence ( $12.5 \text{ J/cm}^2$  – the highest used in this study) can increase the crystallinity of the material as also observed in thin film deposition [44]. Based on the EDX and UV-VIS absorption measurements presented above, we associated the observed diffraction line with the magnetite structure although the XRD pattern of cobalt ferrite is very similar to what was recorded in this study. We suppose that the cobalt ions which should be found in the octahedral sites were replaced by  $\text{Fe}^{3+}$  ions and settled as impurities at crystallite boundaries. Although the  $42^\circ$  diffraction line can easily be associated with the (400) line of the  $\text{Fe}_3\text{O}_4$  structure, the narrower nature of this peak compared to the ones found at  $\sim 35^\circ$  and  $62^\circ$  led us to the conclusion that a more appropriate assignment would be the (200) diffraction line of a second FeO phase [45].

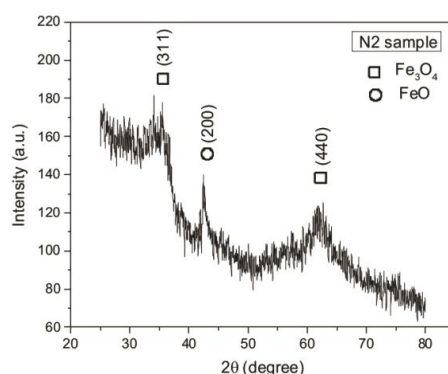


Fig. 3. XRD pattern of the N2 sample obtained using a  $12.5 \text{ J/cm}^2$  fluence

Room temperature magnetic properties of dried nanoparticles were investigated using a vibrating sample magnetometer by applying a 10 kOe maximum magnetic field. The normalized hysteresis loops are presented in Figure 4. All investigated nanoparticles exhibit magnetic characteristics. The values for coercive field ( $H_c$ ) and squareness ( $m_r/m_{\text{max}}$ ) are listed in Table 1. The magnetic properties of the nanoparticles can be influenced by several parameters such as size, shape, crystallinity, chemical composition, presence of impurities at grain boundaries and surface structure [25]. In this study, the highest coercive field and squareness values were found for the N6 sample for which a lower particle size was recorded. One would also expect to obtain similar

values for the N5 sample but the different behavior can be due to differences in chemical composition. EDX measurements revealed an increased Co concentration for the N5 sample whereas an iron overstoichiometry was observed for the N6 nanoparticles. Moreover, the  $H_c$  values can be influenced by the presence of impurities at grain boundaries which act as pinning sites.

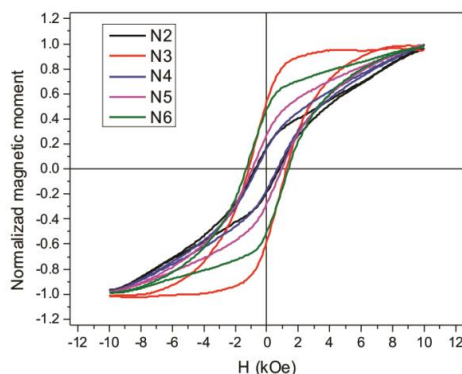


Fig. 4. VSM measurements of magnetic nanoparticles obtained by laser ablation (see Table 1 for assignment of N2-6 samples)

The smallest  $H_c$  and squareness values were found for the N4 sample which has a larger particle size. The decrease of coercive field with particle size indicated that the particles are above the critical size where a monodomain material changes to a multidomain one [46]. The squareness value can give information on the type of intergrain group exchanges [47]. Nanoparticles with  $m_r/m_{\max}$  lower than 0.5 interact by magnetostatic interaction while squareness values higher than 0.5 indicate the presence of exchange – coupled particles. The magnetic results revealed that the obtained particles present a ferromagnetic character which depends on the size and chemical composition.

#### 4. Conclusions

Magnetic nanoparticles were synthesized from cobalt ferrite target by laser ablation in liquid media. TEM images and histograms revealed changes in particle size distribution as the irradiation conditions were varied and ablation liquid was changed. The use of a higher laser energy/pulse and a larger spot size determined the generation of more uniform particles, with narrower size distributions. The same result together with a decrease in particle size was observed when PEG surfactant was added in the ablation liquid. UV-VIS absorption spectra were not significantly influenced by the changes in particle morphology presenting a broad absorption band between 220 nm and 550 nm. The chemical composition obtained by EDX measurements revealed an iron overstoichiometry for most samples. Based on this result, the XRD diffraction lines were associated to iron oxide structures. Magnetic measurement revealed changes in coercive field and squareness with mean particle diameter and chemical composition variation.

#### Acknowledgements

This work was supported by “Alexandru Ioan Cuza” University within “UAIC Grants for young researchers” competition (project code GI-2014-06).

## References

- [1] C.C.H. Lo, *IEEE Trans. Magn.* **43**, 2367 (2007). doi:10.1109/TMAG.2007.892536.
- [2] C. Leroux, M. Bendahan, L. Ajroudi, V. Madigou, N. Mliki, Cobalt Ferrite, *Int. Meet. Chem. Sensors.* (2012) 1119–1121. doi:10.5162/IMCS2012/P1.8.5.
- [3] M.A. Khan, M.M. Alam, M. Naushad, Z.A. Alothman, M. Kumar, T. Ahamad, *Chem. Eng. J.* **279**, 416 (2015). doi:http://dx.doi.org/10.1016/j.cej.2015.05.042.
- [4] H. Arabian Hosseinabadi, M. Edrissi, , *Synth. React. Inorganic, Met. Nano-Metal Chem.* **45**, 1889 (2015). doi:10.1080/15533174.2014.900630.
- [5] P.N. Anantharamaiah, P.A. Joy, *J. Mater. Sci.* **50**, 6510 (2015) doi:10.1007/s10853-015-9211-x.
- [6] K. Mohanraju, V. Sreejith, R. Ananth, L. Cindrella, *J. Power Sources.* **284**, 383 (2015). doi:10.1016/j.jpowsour.2015.03.025.
- [7] E. Fantechi, C. Innocenti, M. Albino, E. Lottini, C. Sangregorio, *J. Magn. Magn. Mater.* **380**, 1 (2014). doi:10.1016/j.jmmm.2014.10.082.
- [8] A. Akbarzadeh, M. Samiei, S. Davaran, *Nanoscale Res. Lett.* **7**, 1 (2012) doi:10.1186/1556-276X-7-144.
- [9] X. Liu, S. Liu, M. Han, L. Zhao, H. Deng, J. Li, Y. Zhu, L. Krusin-Elbaum, S. O'Brien, *Nanoscale Res. Lett.* **8**, 1 (2013).
- [10] A. Lopez-Santiago, H.R. Grant, P. Gangopadhyay, R. Voorakaranam, R. A. Norwood, N. Peyghambarian, *Opt. Mater. Express.* **2**, 978 (2012). doi:10.1364/OME.2.000978.
- [11] A.B. Rajput, S.J. Rahaman, G. Sarkhel, M.K. Patra, S.R. Vadera, P.M. Singru, Y. Yagci, N. N. Ghosh, *J. Appl. Polym. Sci.* **128**, 3726 (2013). doi:10.1002/app.38426.
- [12] A. Lopez-Santiago, P. Gangopadhyay, J. Thomas, R.A. Norwood, A. Persoons, N. Peyghambarian, *Appl. Phys. Lett.* **95**, 143302 (2009). doi:10.1063/1.3238553.
- [13] Y. Vitta, V. Piscitelli, A. Fernandez, F. Gonzalez-Jimenez, J. Castillo, *Chem. Phys. Lett.* **512**, 96 (2011)–98. doi:10.1016/j.cplett.2011.07.020.
- [14] S. Barcikowski, G. Compagnini, *Phys. Chem. Chem. Phys.* **15**, 3022 (2013). doi:10.1039/c2cp90132c.
- [15] H. Zeng, X.-W. Du, S.C. Singh, S. A. Kulinich, S. Yang, J. He, W. Cai, *Adv. Funct. Mater.* **22**, 1333 (2012). doi:10.1002/adfm.201102295.
- [16] A. Kebede, A.K. Singh, P.K. Rai, N.K. Giri, A.K. Rai, G. Watal, A. V. Gholap *Lasers Med. Sci.* **28**, 579 (2013). doi:10.1007/s10103-012-1106-3.
- [17] T. Nishi, A. Takeichi, H. Azuma, N. Suzuki, T. Hioki, T. Motohiro, *J. Laser Micro Nanoeng.* **5**, 192 (2010) doi:10.2961/jlmm.2010.03.0002.
- [18] M. Gracia-Pinilla, M. Villanueva, N.A. Ramos Delgado, M.F. Melendrez, J. Menchaca-Arredondo, *Dig. J. Nanomater. Biostructures.* **9**, 1389 (2014).
- [19] T. Tsuji, T. Hamagami, T. Kawamura, J. Yamaki, M. Tsuji, *Appl. Surf. Sci.* **243**, 214 (2005). doi:10.1016/j.apsusc.2004.09.065.
- [20] F. Stokker-Cheregi, T. Acsente, I. Enculescu, C. Grisolia, G. Dinescu, *Dig. J. Nanomater. Biostructures.* **7**, 1569 (2012).
- [21] A.R. Sadrolhosseini, S.A. Rashid, A.S.M. Noor, A. Kharazmi, L.A. Mehdipour *Dig. J. Nanomater. Biostructures.* **10**, 1009 (2015).
- [22] H.R. Dehghanpour, L. Delshad, *J. Laser Appl.* **26**, 022008 (2014). doi:10.2351/1.4866677.
- [23] R. Nawathey-Dikshit, S.R. Shinde, S.B. Ogale, S.D. Kulkarni, S.R. Sainkar, S.K. Date, *Appl. Phys. Lett.* **68**, 3491 (1996). doi:10.1063/1.115768.
- [24] H. Zhang, C. Liang, Z. Tian, G. Wang, W. Cai, *J. Phys. Chem. C.* **114**, 12524 (2010).
- [25] P. Maneeratanasarn, T. Van Khai, S.Y. Kim, B.G. Choi, K.B. Shim, *Phys. Status Solidi Appl. Mater. Sci.* **210**, 563 (2013)–569. doi:10.1002/pssa.201228427.
- [26] H.S. Desarkar, P. Kumbhakar, A.K. Mitra, *Appl. Nanosci.* **2**, 285 (2012). doi:10.1007/s13204-012-0106-8.
- [27] G. Dascalu, G. Pompilian, B. Chazallon, V. Nica, O.F. Caltun, S. Gurlui, C. Focsa, *Appl. Phys. A.* **110**, 915 (2012). doi:10.1007/s00339-012-7196-8.
- [28] G. Dascalu, G. Pompilian, B. Chazallon, O.F. Caltun, S. Gurlui, C. Focsa, *Appl. Surf. Sci.* **278**, 38 (2013). doi:10.1016/j.apsusc.2013.02.107.

- [29] G. Bulai, L. Diamandescu, I. Dumitru, S. Gurlui, M. Feder, O.F. Caltun, J. Magn. Magn. Mater. **390**, 123 (2015). doi:10.1016/j.jmmm.2015.04.089.
- [30] P. Liu, W. Cai, H. Zeng, J. Phys. Chem. C. **112**, 3261 (2008). doi:10.1021/jp709714a.
- [31] L. Franzel, M.F. Bertino, Z.J. Huba, E.E. Carpenter, Appl. Surf. Sci. **261**, 332 (2012). doi:10.1016/j.apsusc.2012.08.010.
- [32] L. Khanna, N.K. Verma, Phys. B Condens. Matter. **427**, 68 (2013). doi:10.1016/j.physb.2013.05.040.
- [33] H. Kavas, A. Baykal, M.S. Toprak, Y. Köseoğlu, M. Sertkol, B. Aktaş, J. Alloys Compd. **479**, 49 (2009). doi:10.1016/j.jallcom.2009.01.014.
- [34] S. Esir, R. Topkaya, A. Baykal, Ö. Akman, M.S. Toprak, J. Inorg. Organomet. Polym. Mater. **24**, 424 (2014). doi:10.1007/s10904-013-9997-4.
- [35] A.F.M.Y. Haider, S. Sengupta, K.M. Abedin, A.I. Talukder, Appl. Phys. A Mater. Sci. Process. **105**, 487 (2011). doi:10.1007/s00339-011-6542-6.
- [36] M.A. Sobhan, M. Ams, M.J. Withford, E.M. Goldys, J. Nanoparticle Res. **12**, 2831 (2010). doi:10.1007/s11051-010-9868-7.
- [37] A. Miotello, P.M. Ossi, Laser-Surface Interactions for New Materials Production, Springer Series in Material Science, 2010. doi:10.1007/978-3-642-03307-0.
- [38] D.H.A. Blank, R.P.J. IJsselsteijn, P.G. Out, H.J.H. Kuiper, J. Flokstra, H. Rogalla, Mater. Sci. Eng. B. **B13**, 67 (1992). doi:10.1016/0921-5107(92)90106-J.
- [39] A. Hahn, S. Barcikowski, B.N. Chichkov, J. Laser Micro/Nanoengineering. **3**, 73 (2008). doi:10.2961/jlmn.2008.02.0003.
- [40] E.M. Rajesh, K. Shamili, R. Rajendran, M. Elango, S.R.M. Shankar, Adv. Sci. Eng. Med. **6**, 268 (2014). doi:10.1166/ asem.2014.1503.
- [41] V. Amendola, P. Riello, M. Meneghetti, J. Phys. Chem. C. **115**, 5140 (2011). doi:10.1021/jp109371m.
- [42] K. Klačanová, P. Fodran, P. Šimon, P. Rapta, R. Boča, V. Jorík, M. Miglierini, E. Kolek, L. Čaplovič, J. Chem. 2013 (2013). doi:10.1155/2013/961629.
- [43] R. Asokarajan, K. Neyvasagam, A. Milton Franklin Benial, Int. J. Curr. Res. **5**, 113 (2013).
- [44] W. Liu, C. Wen, X. Zhang, J. Liu, J. Liang, X. Long, Phys. Scr. **90**, 035402 (2015). doi:10.1088/0031-8949/90/3/035402.
- [45] A. Lak, M. Kraken, F. Ludwig, A. Kornowski, D. Eberbeck, S. Sievers, F. L. Litterst, H. Weller, M. Schilling, Nanoscale. **5**, 12286 (2013). doi:10.1039/c3nr04562e.
- [46] D.S. Mathew, R.-S. Juang, Chem. Eng. J. **129**, 51 (2007). doi:10.1016/j.cej.2006.11.001.
- [47] M. Goodarz Naseri, E.B. Saion, H. Abbastabar Ahangar, A.H. Shaari, M. Hashim, J. Nanomater. 2010 (2010). doi:10.1155/2010/907686.